Journal of MATERIALS RESEARCH

Article
DOI:10.1557/s43578-023-01258-5

Investigation of photodetector and photovoltaic properties of H_2Pc/CuO and H_2Pc/ITO junctions produced with modified H_2Pc

Fatih Unal[1,a)], Sitki Aktas[2,a)], Mustafa Sukru Kurt[3], Mümin Mehmet Koc[4,5], Tayfun Arslan[6], Burhan Coskun[5], Mahmut Gur[7]

[1] Central Research Laboratories, Application and Research Centre, GRUMLAB, Giresun University, 28200 Giresun, Turkey
[2] Department of Mechanical Engineering, Faculty of Engineering, Giresun University, Giresun, Turkey
[3] Department of Fundamental Science, Science Faculty, Erzurum Technical University, Erzurum, Turkey
[4] Department of Medical Service and Techniques, School of Medical Service, Kirklareli University, Kirklareli, Turkey
[5] Department of Physics, Faculty of Science and Literature, Kirklareli University, Kirklareli, Turkey
[6] Department of Chemistry, Faculty of Science, Giresun University, Giresun, Turkey
[7] Department of Forest Industrial Engineering, Faculty of Forestry, Kastamonu University, 37100 Kastamonu, Turkey
[a)] Address all correspondence to these authors. e-mails: fatih.unal@giresun.edu.tr; sitki.aktas@giresun.edu.tr

Received: 20 April 2023; accepted: 29 November 2023; published online: 18 December 2023

In this work, it was aimed to provide an alternative to organic-based photodiode detectors (OPDs), solar cell with the modified H_2Pc organic thin film heterojunctions. For this purpose, the modified H_2Pc organic thin film was grown on ITO/glass and CuO_x/ITO/glass substrates via thermal evaporation method and their optoelectronic properties were compared with each other and other organic-based devices. The crucial optical parameters of the fabricated heterojunctions were determined in the wavelengths range of 300–800 nm. In order to perform electrical characterisation, Ag metal contacts were grown on the heterojunctions and Ag/H_2Pc/ITO/Ag and Ag/H_2Pc/CuO_x/Ag devices were fabricated. Diode, photovoltaic and photodetector parameters of the fabricated devices were investigated in the applied potential of ± 3 V under dark and several light intensities. Ultimately, it can be stated that the fabricated devices may offer an alternative to OPDs and organic-based solar cell.

Introduction

The use of organic semiconductors in a wide range of new technologies has attracted intense interest due to their structural and functional tunability. The combination of the film-forming ability of organics and the superior electrical properties of inorganic materials makes it possible to develop a new class of semiconductor devices which can be used as flexible electronics and optoelectronics and photovoltaics [1, 2]. Among these, using organic materials as an interface layer at metal–semiconductor (MS) structure would ensure beneficial improvements of the electrical properties of the structure. For instances, symmetrical CuPc organic molecule was coated on a p-Si wafer as an interfacial layer and it was obtained that Al/symmetrical CuPc/p-Si/Al heterojunction could be used as a photodevice or photosensor [3]. The negative differential resistance (NDR) behaviour was investigated on PMItz/ITO junction and it was seen that NDR effect strongly related with light intensity [4]. P3HT/n-Si organic–inorganic hybrid solar cell was fabricated and light dependence of the current transport mechanisms was investigated [2]. Coronene ($C_{24}H_{12}$) thin films were grown on the CdO [5], ZnO [6], Cu-doped ZnO [7] metal oxides structure and optoelectronic properties were analysed. A self-powered PEDOT:PSS/Ga_2O_3 organic–inorganic hybrid heterojunction was investigated with excellent photoelectric properties [8]. Additionally, Phthalocyanine (Pcs) molecules with a two-dimensional conjugated π-electrons system provide a large charge transfer [9]. Thanks to these properties, Pcs and their analogues have been widespreadly used in several technological areas [10, 11]. Especially, the metal-free phthalocyanine (H_2Pc) materials are widely used in photodetectors, solar cells and other optoelectronic devices [12, 13].

Thin film copper oxides produced by several techniques are widely used metal oxide semiconductor in the area of device manufacturing, optoelectronic and photovoltaic applications [14–16]. The oxide phases of copper oxide, which have distinct the optical and electrical properties, can be altered by reactive sputtering during the magnetron sputtering deposition process or by post-deposition annealing at various temperatures under vacuum or atmosphere [14, 17–20]. Hence, in this study, Cu thin film was grown on ITO substrate via magnetron sputtering technique and annealed in oxygen environment under vacuum conditions after deposition. Structural, morphological properties of deposited copper oxide thin film were investigated. Afterwards, unlike the known phthalocyanines, in order to investigate the interface layer performance of metal free-Pcs have chalcone, which π-bridge consists of *α*, β unsaturated carbonyl unit which is responsible for intramolecular charge transfer, the H_2Pc organic molecules was deposited as a thin film on commercial ITO and magnetron sputtered CuO_x surfaces via physical vapour deposition (PVD) method. Optical characterisation of H_2Pc/ITO and H_2Pc/CuO_x/ITO heterojunctions was examined. Eventually, with growing Ag contacts on both the heterojunctions, Ag/H_2Pc/ITO/Ag and Ag/H_2Pc/CuO_x/Ag devices were fabricated and photodiode, photodetector and photovoltaic characteristics of these devices were examined in detail.

Results and discussion

Structural, morphological and optical characterisation of CuO_x thin film

The XRD pattern of CuO_x thin film is presented in Fig. 1(a). It can be clearly observed that post-annealing at 200 °C during 30 min led to the copper thin film crystallised in the form of CuO_2 and cupric oxide (CuO). The most intense peak at 2*θ* of 35.22° represents the crystallographic reflection of (002) plane of monoclinic CuO with the space group C12/c1(15) and the lattice constant of a = 4.6839 Å, b = 3.4734 Å, c = 5.1226 Å and *β* = 98.730° (entry # 96-901-5888). Furthermore, 2 *θ* values of 29.15°, 31.43°, 36.03°, 50.62° and 60.16° indicate orthorhombic CuO_2 with the (200), (400), (111), (131) and (440) planes, respectively (entry # 96-152-1321). Lattice parameters of CuO_2 are given as *a* = 11.4 Å, *b* = 7.30 Å, *c* = 2.73 Å and *Z* = 4 with the space group F222(22). The rest of the labelled peaks reveal the ITO because of the use of ITO as the substrate. Previous studies indicate that the formation of copper oxide phases depended on annealing temperature, time and amount of injected O_2. For instance, Dolai et al. [14] reported that XRD pattern of a thin film deposited via reactive magnetron sputtering of Cu target with the Ar and O_2 ratio of 60:40 at 573 K revealed metallic Cu peaks and by increasing the temperature to 623 K only CuO

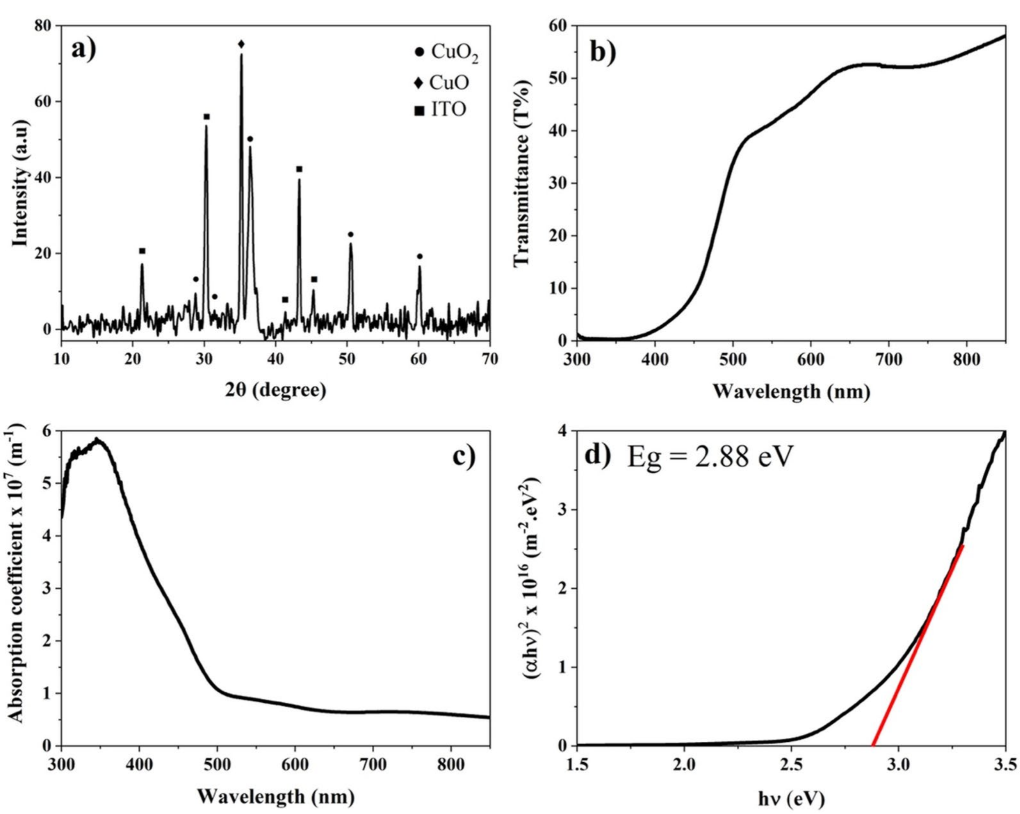

Figure 1: (a) XRD pattern, (b) transmittance, (c) absorption coefficient, (d) energy band gap for post-annealed CuO_x thin film deposited on ITO/glass substrate.

peaks exist. However, the XRD measurement reveals that two copper oxide phases coexist formed in the film and metallic Cu was not obtained. Hence, the XRD result indicates that magnetron sputtered copper film fully oxidised under oxygen environment via post-deposition annealing process at 473 K under high vacuum conditions and crystallised as two copper oxide phases.

Figure 1(b) illustrates the transmittance versus wavelength plot of CuO_x thin film deposited on ITO/glass substrate. Transmittance was determined via its relationships with absorbance ($A = -logT$) with the formula of $T = (1 - R)^2 \exp(-A)$ which neglects the multiple reflections [21]. The transmittance values of the CuO_x thin film in the visible region initially sharply increased from 2.37 to 38.1% with increasing the wavelength from 400 to 530 nm, thereafter, it reached to 53.76% at 780 nm. Figure 1(c) displays the absorption coefficient of the deposited CuO_x thin film, determined via the equation of $\alpha = 2.303\ A/d$, where A and d refer to the absorbance and the thickness of the film [22], respectively, versus wavelength. The strongest absorption peak of CuO_x thin film was obtained at 370 nm with the value of 5.8×10^7 m^{-1}. As illustrated in Fig. 1(d), the energy band gap (Eg) value of the CuO_x thin film was identified by extrapolating the linear portion of $(\alpha h\nu)^2$ to the photon energy ($\alpha h\nu$) axis. Figure 2(d) was extracted from the Tauc plot method [23] which utilises the absorption coefficient (α)-related equation, $\alpha (h\nu) \approx (h\nu - E)^n$, where n is 1/2 for direct allowed transition [24, 25]. It can be noted that energy band gap of the CuO_x thin film deposited on ITO/glass substrate was measured as 2.88 eV.

Morphology of the CuO_x thin film was evaluated from the top-view SEM micrographs, which were taken at 10 k, 20 k and 40 k magnifications and are shown in Fig. 2(a)–(c), respectively. Low-magnification image displayed in Fig. 2(a) shows that CuO_x thin film homogenously formed on ITO/glass. It might be observed from high-magnification images that the thin film has rough surface with nanoscale particles formed on top of the film. While the diameter of the nanoscale particles was denser in the size range of 100–300 nm, upto 800 nm particles also exist as shown in Fig. 2(c). EDX-mapping image [shown in Fig. 2(d)] demostrates that the deposited copper film homogenously oxidised thanks to post-deposition annealing process and this supports the XRD result presented in Fig. 1(a). Additionally, the proportions of elemental weight of Cu and O were measured as 79.45 and 20.55, respectively.

Optical characterisation of H_2Pc/ITO and H_2Pc/CuO_x/ITO heterojunctions

Optical characterisation of fabricated heterojunctions is an important aspect to establish their compatibilities of optoelectronic applications. Hence, crucial optical parameters such as absorption coefficient (α), optical transmittance ($T\%$), reflectance ($R\%$), energy band gap (E_g), extinction coefficient (k),

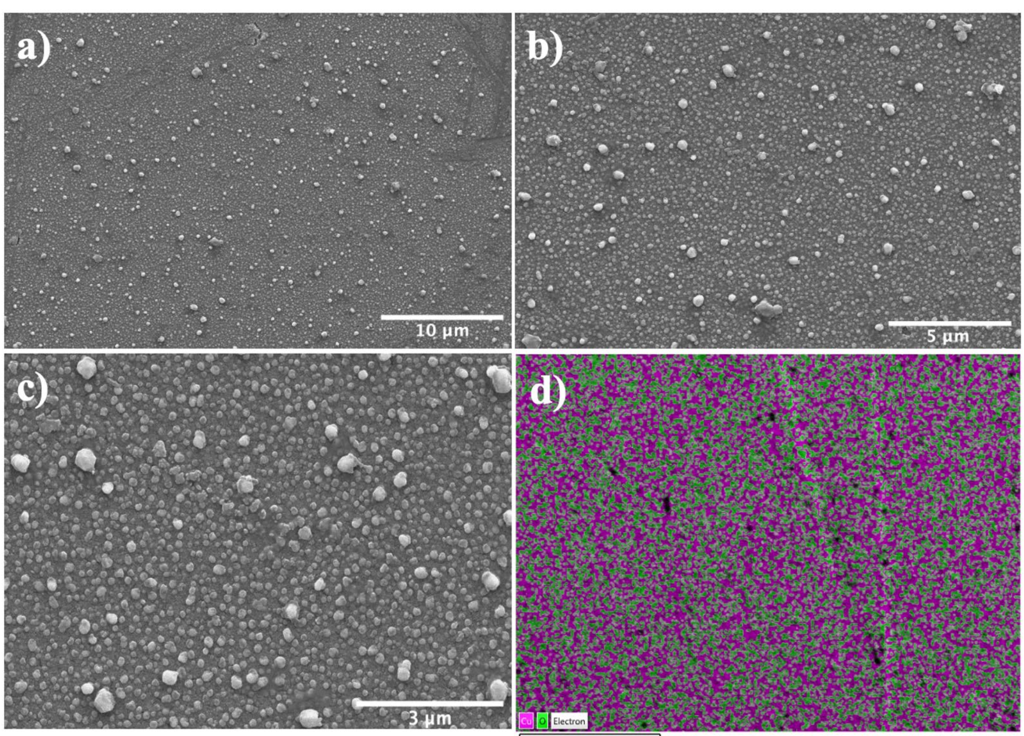

Figure 2: SEM micrograph of CuO_x thin film (a) at 10 k, (b) 20 k and (c) 40 k magnifications. (d) EDX-mapping image of CuO_x thin film (Purple and green indicate the copper and oxygen, respectively).

Journal of Materials Research ■ Volume 39 ■ Issue 4 ■ February 2024 ■ www.mrs.org/jmr

refractive index (n), optical conductivity (σ), real dielectric constant (ε_r and imaginary dielectric constants (ε_i), and dielectric loss ($\varepsilon_i/\varepsilon_r$) [26–29] of H_2Pc/ITO and H_2Pc/CuO_x/ITO heterojunctions were deeply evaluated between the 300 and 800 nm wavelength range.

The transmittance of H_2Pc/ITO and H_2Pc/CuO_x/ITO heterojunctions as a function of wavelength are illustrated in Fig. 3(a). While the transmittance of H_2Pc/ITO was fluctuated between the values of 65% and 93% and reached its maximum value of 93% at 480 nm, that of H_2Pc/CuO_x/ITO started to increase after 400 nm and reached its maximum value 38% at 600 nm. The big difference between the transmittance values is due to the CuO_x thin film which has 47% transmittance vales at 600 nm as shown in Fig. 1(b). The strongest absorption coefficients of H_2Pc/ITO and H_2Pc/CuO_x/ITO were calculated as 2.2×10^6 m^{-1} at 390 nm and 1.7×10^7 m^{-1} at 340 nm, respectively [see Fig. 3(b)]. While absorption coefficients of H_2Pc/CuO_x/ITO heterojunction sharply decreased to 4.2×10^6 m^{-1} till 510 nm and thereafter approximately stabilised, for H_2Pc/ITO this was slightly fluctuated with increasing the wavelength. It can be clearly seen that there is an inverse correlation between $T\%$ and α in both the heterojunctions and this is because of the incident photons on the sample in the region with the lowest $T\%$ value have undergone maximum absorption. It is obvious that the H_2Pc/CuO_x/ITO heterojunction had lower $T\%$ values and higher α values than the H_2Pc/ITO heterojunction. This can be explained by the fact that the CuO_x layer plays a crucial role in photon absorption. Reflectance of both the heterojunctions was defined via the equation of $R=1-(T/\exp(-A))^{1/2}$ [30] as a function of wavelength and is demonstrated in Fig. 3(c). The reflectance value of H_2Pc/ITO heterojunctions varied between 2.1 and 4.7% due to its high transmittance. Strongest reflectance of H_2Pc/CuO_x/ITO was obtained at 310 nm with the value of 9.7% and it decreased to 6.7% at 800 nm. Furthermore, direct energy band gap values of the heterojunctions are displayed in Fig. 3(d) and they were determined as 2.66 eV and 2.77 eV for H_2Pc/ITO and H_2Pc/CuO_x/ITO heterojunctions, respectively. This difference of the direct energy band gap of the H_2Pc thin film is related to the substrate on which it is amplified. Organic-based thin films may exhibit different behaviours on different substrates due to their nature [5–7, 31].

Figure 3(e) and (f) shows the variation of extinction coefficient ($k=\frac{\lambda\cdot\alpha}{4\pi}$) and refractive index ($n=\frac{1+R}{1-R}+\sqrt{\frac{4R}{1-R^2}-k^2}$) for both the heterojunctions with wavelengths. It is seen that the k value of the H_2Pc/CuO_x/ITO heterojunction increased with the increase of wavelength, reached a maximum value of 0.45 at 350 nm, then rapidly decreased and had a value of 0.17 at 500 nm and then slightly increased. Besides, k value of the H_2Pc/ITO heterojunction fluctuated at short wavelength region and reached its maximum value of 0.09 at 800 nm by increasing slowly. While n values of H_2Pc/CuO_x/ITO heterojunction exhibited generally

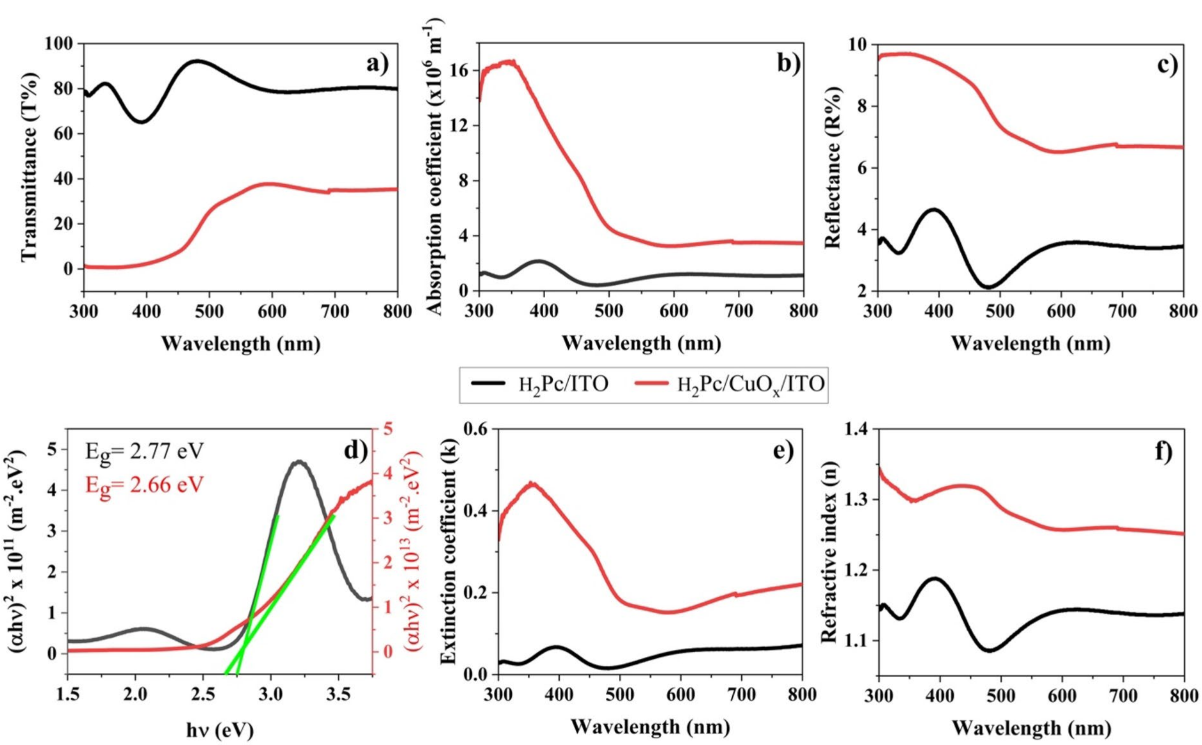

Figure 3: (a) Transmittance, (*b*) absorption coefficient, (*c*) reflectance of H_2Pc/ITO and H_2Pc/CuO_x/ITO heterojunctions as a function of wavelength. (*d*) (ahv^2versus (hv plot for both the heterojunctions, (*e*) extinction coefficient (k) and (*f*) Refractive index (n) versus wavelength graphs of H_2Pc/ITO and H_2Pc/CuO_x/ITO heterojunctions.

Journal of Materials Research ■ Volume 39 ■ Issue 4 ■ February 2024 ■ www.mrs.org/jmr

decreasing behaviour with increasing the wavelength with an exception of small fluctuation around 430 nm, for H_2Pc/ITO heterojunction this peaked at 390 nm with the value of 1.19 and decreased to 1.09 at 430 nm and reached its beginning value with increasing the wavelength. It is also obvious that the H_2Pc/CuO_x/ITO heterojunction had higher k and n values than the H_2Pc/ITO heterojunction at all wavelengths and this became more pronounced especially in the absorption region. Generally, higher k and n values mean more absorption of light incident on heterojunctions and over-absorbed photons lead to overproduction of photogenerated carriers, which is very important in optoelectronic applications.

The optical conductivity ($\sigma = \alpha nc/4\pi$), imaginary dielectric constant ($\varepsilon_i = 2nk$), real dielectric constant ($\varepsilon_r = n^2 - k^2$) and dielectric loss ($\varepsilon_i/\varepsilon_r$) are the important parameters of the electronic excitation profile of the heterojunctions, and are given as a function of wavelength in Fig. 4. The highest values of σ, ε_r, ε_i and $\varepsilon_i/\varepsilon_r$ for H_2Pc/CuO_x/ITO heterojunction were obtained as 5.1×10^{15} at 360 nm, 1.65 at 480 nm, 1.2 at 360 nm and 0.9 at 370 nm, respectively. Furthermore, they were 7×10^{14} at 400 nm, 1.4 at 400 nm, 0.19 at 400 nm and 0.11 at 400 nm for H_2Pc/ITO heterojunction, respectively.

Electrical characterisation of Ag/H_2Pc/ITO/Ag and Ag/H_2Pc/CuO_x/Ag heterojunctions

Traditional I–V characterisation is the most common used method to investigate the electrical properties of semiconductors. Current conduction mechanism in semiconductors is determined via I–V characteristics. Hence, electrical characterisations of Ag/H_2Pc/ITO/Ag and Ag/H_2Pc/CuO_x/Ag devices were investigated in the potential range of ± 3 V under dark and 20, 40, 60, 80 and 100 $mW.cm^{-2}$ light intensities. Semilogarithmic I–V plots of Ag/H_2Pc/ITO/Ag and Ag/H_2Pc/CuO_x/Ag devices are shown in Fig. 5(a) and (b), respectively. It might be noted that both the heterojunctions exhibited asymmetric behaviours at low voltage region and series resistance effect was observed for the heterojunctions towards the high voltage region. While series resistance effect in the Ag/H_2Pc/ITO/Ag device was observed at the voltage values greater than 0.46 V, this was monitored at voltage region higher than 0.3 V in the Ag/H_2Pc/CuO_x/Ag device. The variations of the rectification ratio ($RR = I_{forward}/I_{reverse}$) values of the Ag/$H_2Pc$/ITO/Ag and Ag/$H_2Pc/CuO_x$/Ag devices under dark and light intensities in accordance with the applied potentials are displayed in Fig. 5(c) and (d), respectively. It is clear that RR values for

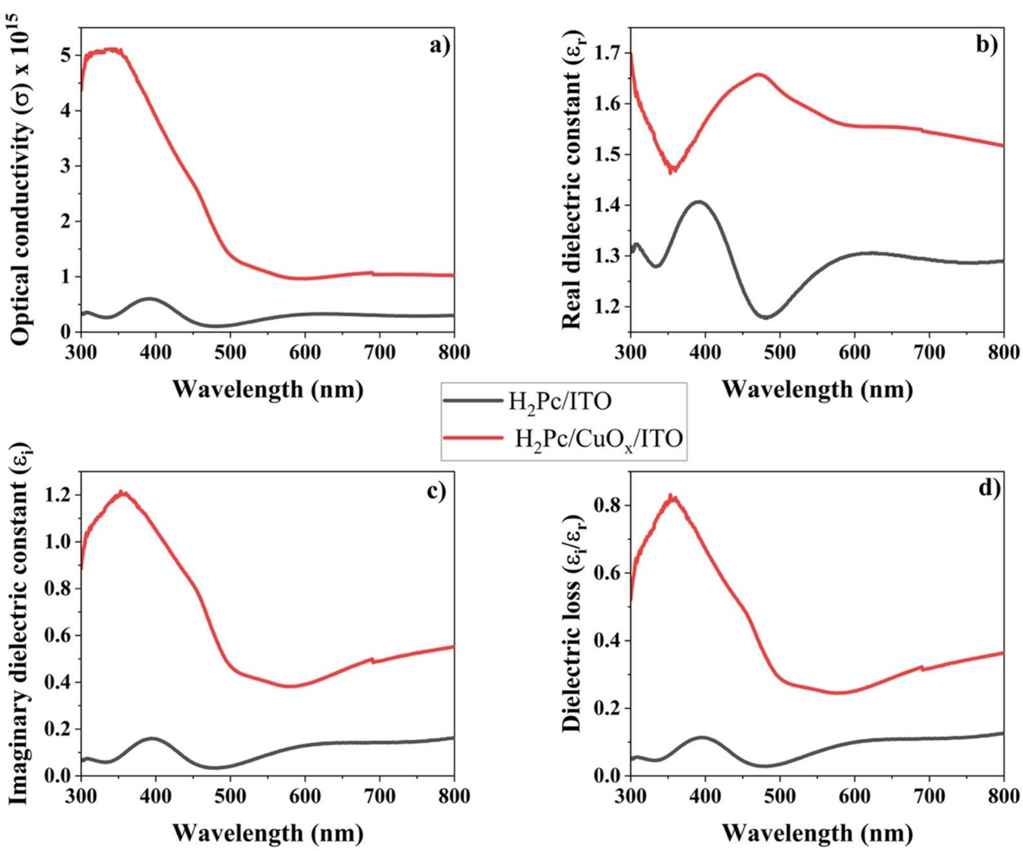

Figure 4: (a) Optical conductivity, (b) real dielectric constant, (c) imaginary dielectric constant and (d) dielectric loss of the heterojunctions as a function of wavelength.

Journal of Materials Research ■ Volume 39 ■ Issue 4 ■ February 2024 ■ www.mrs.org/jmr

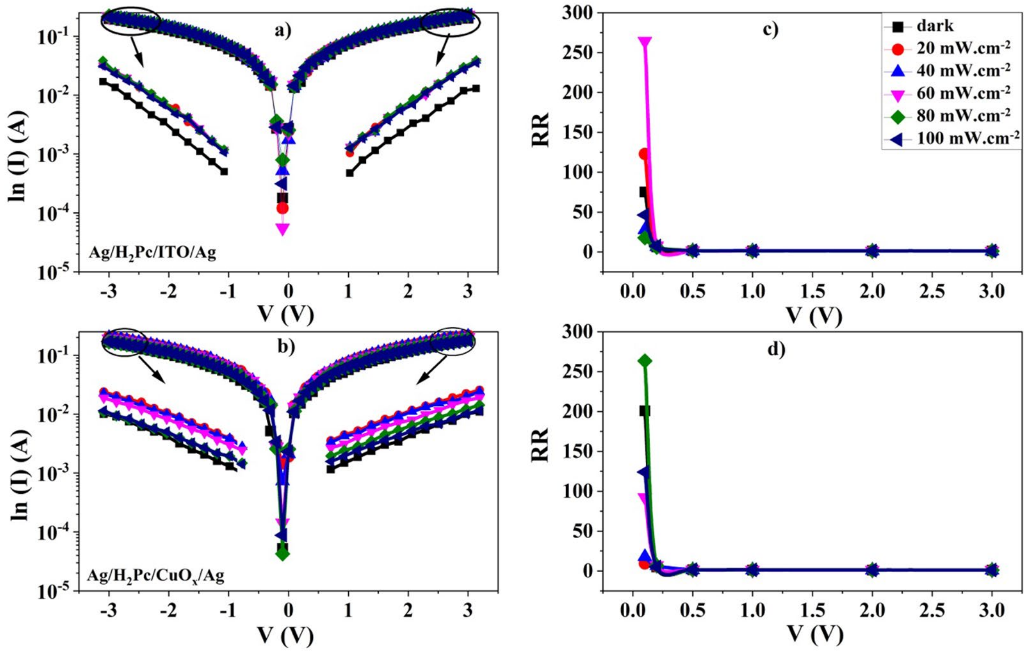

Figure 5: Semilogarithmic *I–V* plot of (a) Ag/H_2Pc/ITO/Ag (b) Ag/H_2Pc/CuO_x/Ag devices. The RR against V graph of (c) Ag/H_2Pc/ITO/Ag (b) Ag/H_2Pc/CuO_x/Ag heterojunctions.

both the devices exponentially decreased with the increase of applied voltage. While the RR values of Ag/H_2Pc/ITO/Ag device at 0.1 V under dark environment was about 75, this was 1.01 at 3 V. Similarly, while the RR values of Ag/H_2Pc/CuO_x/Ag device at 0.1 V under dark environment was approximately 200, this was 1.07 at 3 V. The decrease of RR values in accordance with the applied voltage can be explained with the charge accumulation at the interface and narrowing depletion region [32–34]. In addition, slow electron and hole mobility can be associated with the becoming of low RR value at high voltage values [35].

Electrical characterisation of *I–V* characteristic of heterojunctions exhibiting asymmetric behaviour can be analysed by thermionic emission theory [36] or by using the Cheung&Cheung functions [37] as well. Table 1 shows the variation of electrical parameters such as diode ideality factor (n), barrier height (ϕ_b), series resistance (R_s) and reverse saturation current (I_0) calculated by different methods, depending on light intensity. While the ideality factor of Ag/H_2Pc/ITO/Ag and Ag/H_2Pc/CuO_x/Ag devices calculated by traditional method took values between 14.82 and 13.62 and 13.20 and 10.34, respectively, these calculated by Cheung&Cheung functions took values between 3.92 and 1.02 and 4.05 and 1.40. ϕ_b values of Ag/H_2Pc/ITO/Ag and Ag/H_2Pc/CuO_x/Ag devices determined by the traditional method ranged between 0.428 and 0.424 eV, 0.436 and 0.430 eV, respectively. Besides, ϕ_b values of Ag/H2Pc/ITO/Ag and Ag/H2Pc/CuO/Ag devices determined from Cheung&Cheung functions ranged between 0.09 and 0.34 eV and 0.11 and 0.30 eV, respectively. It can be stated that n and ϕ_b values calculated by two different methods exhibited similar behaviours depending on light intensity, however, there were differences in the calculated values. These differences can be issued due to difference of the I–V regions used for calculations. Additionally, as a result of the increase of light intensity, while n values of both the heterojunctions decreased, ϕ_b values increased by exhibiting opposite behaviour which has been obtained in previous studies [38–40]. These changes of n and ϕ_b values under light intensity occurred in a fluctuating manner in both the heterojunctions as well and these could be attributed to the generation/separation of electron–hole pairs and reordering and restructuring molecular structures on the surface [38, 41]. n values of both the devices are far from the ideal diode ($n = 1$) [42] but it is possible to encounter many studies involving heterojunctions where n values are greater than 1 [5, 43, 44]. There are several reasons that lead to n values greater than 1, can be listed as the regeneration and coupling of electron–hole pairs, distribution of interfacial charges, expansion of depletion layer, series resistance and non-homogeneous distribution of layers [41, 42, 45, 46].

Figure 6(a) and (b) illustrates the variation of ϕ_b values calculated via Cheung& Cheung functions as a function of n values of Ag/H_2Pc/ITO/Ag and Ag/H_2Pc/CuO_x/Ag devices. Also, the graphs of the ϕ_b values determined by traditional method against n values of Ag/H_2Pc/ITO/Ag and Ag/H_2Pc/CuO_x/Ag devices are displayed in Fig. 6(c) and (d). The equations in which ϕ_b values calculated from Cheung&Cheung functions of Ag/H_2Pc/ITO/Ag and Ag/H_2Pc/CuO_x/Ag devices depend on n are

TABLE 1: Diode parameters of Ag/H_2Pc/ITO/Ag and Ag/H_2Pc/CuO_x/Ag devices.

Light intensity ($mW\ cm^{-2}$)	Cheung and Cheung functions: $dV/d\ln I$–I		$H(I)$–I		Traditional method: $\ln(I)$–V			Ohm's law $\frac{\partial V}{\partial I}$
Ag/H_2Pc/ITO/Ag	n	R_s (Ω)	ϕ_b (eV)	R_s (Ω)	n	ϕ_b (eV)	I_0 (A)	R_s (Ω)
Dark	3.92	16.74	0.09	8.19	14.62	0.420	1.02×10^{-3}	14.88
20	3.10	13.59	0.11	7.41	14.06	0.425	1.15×10^{-3}	13.16
40	2.33	13.83	0.14	7.81	14.27	0.424	1.20×10^{-3}	13.13
60	2.50	13.87	0.14	7.47	14.82	0.424	1.20×10^{-3}	13.16
80	1.02	15.04	0.34	7.71	13.69	0.425	1.15×10^{-3}	13.12
100	2.41	14.56	0.14	7.75	14.07	0.424	1.19×10^{-3}	13.26
Ag/H_2Pc/CuO_x/Ag	n	R_s (Ω)	ϕ_b (eV)	R_s (Ω)	n	ϕ_b (eV)	I_0 (A)	R_s (Ω)
Dark	4.05	17.65	0.11	9.46	11.24	0.436	7.52×10^{-3}	16.85
20	2.27	16.21	0.17	7.28	11.20	0.430	9.52×10^{-3}	14.03
40	1.83	14.74	0.21	7.21	10.88	0.430	9.41×10^{-3}	14.22
60	3.89	13.67	0.11	7.19	13.20	0.429	1×10^{-2}	14.96
80	3.58	15.29	0.12	7.89	10.36	0.435	7.82×10^{-3}	15.94
100	1.40	17.63	0.30	8.81	10.34	0.436	7.67×10^{-3}	16.7

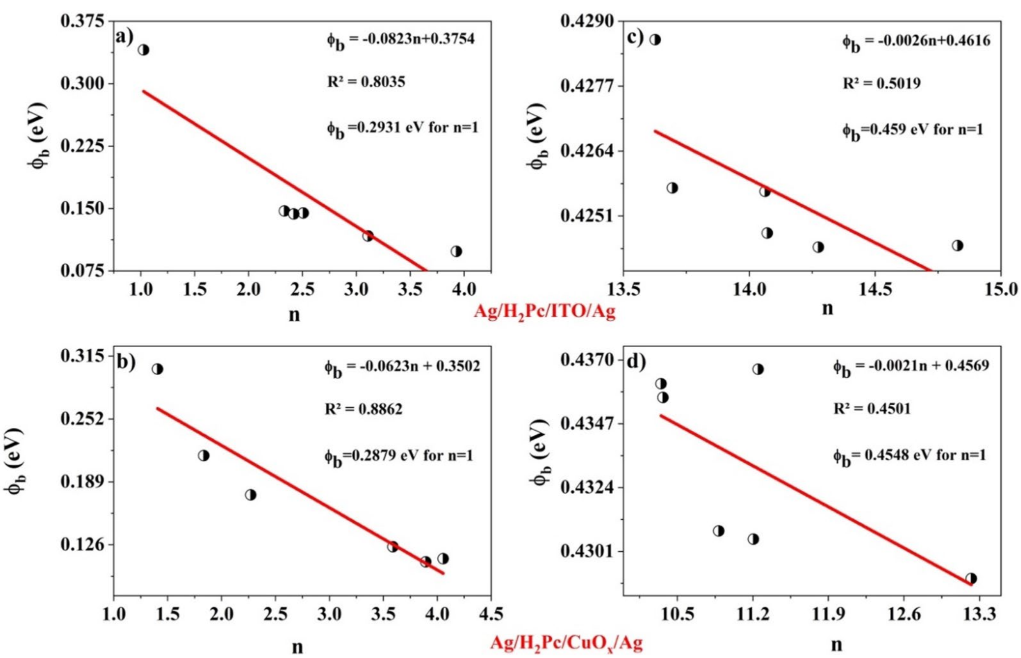

Figure 6: The graphs of the ϕ_b values calculated via Cheung& Cheung functions versus n values of (a) Ag/H_2Pc/ITO/Ag (b) Ag/H_2Pc/CuO_x/Ag devices. The graphs of the ϕ_b values calculated by the traditional method against to n values of (c) Ag/H_2Pc/ITO/Ag d) Ag/H_2Pc/CuO_x/Ag devices.

$\phi_b = -0.0823n + 0.3754$ and $\phi_b = -0.0623n + 0.3502$ and for $n = 1$, ϕ_b values are 0.2931 eV and 0.2879 eV, respectively. Additionally, equations of ϕ_b value calculated by traditional method for Ag/H_2Pc/ITO/Ag and Ag/H_2Pc/CuO_x/Ag devices are $\phi_b = -0.0026n + 0.4616$ and $\phi_b = -0.0021n + 0.4569$ and for $n = 1$, ϕ_b values are 0.4590 eV and 0.4501 eV, respectively. It can be seen that ϕ_b values linearly depend on n values as illustrated in Fig. 6. Lowest and highest ϕ_b value for n = 1 was observed in the $Ag/H_2Pc/ITO/Ag$ and $Ag/H_2Pc/CuO_x/Ag$ devices, respectively. It can also be stated that high ϕ_b values were obtained at low n values for both the heterojunctions. In general, charge carrier mobility increases with the increase of light intensity. Hence, due to the movement of these carriers, barrier height might increase and ideality factor might decrease. That is, as the light intensity increases, more electrons would have enough energy to overcome higher barrier [47]. Similar situations were studied by Monch et al. [48], Akkilic et al. [49] and Schmitsdorf et al. [50]. Additionally, the relationship between the high barrier height and low fidelity factor can be attributed as the bias dependence of the saddle point potential of an inhomogeneous barrier [49].

Series resistance (R_s) is a very crucial parameter for diodes and it significantly affects the device quality and performance [51]. The changes of R_s values depending on light intensity were determined by Cheung&Cheung functions and ohm's law ($R_j = \frac{\partial V}{\partial I}$). It is obtained that R_s values of fabricated devices were found to be quite low compared to the literature [40, 52–54]. R_s values decreased with increasing light intensity in both the devices and the lowest R_s value was observed in $Ag/H_2Pc/ITO/Ag$ device. The decrease in R_s values can be explained with the increase in electrical conductivity under light [39]. Besides, I_0 values calculated by traditional method exhibited increasing tendency with the increase of light intensity. The minority carrier concentration also increased due to photon absorption, and similar situation has been observed by many researchers [55–57]. While I_0 of $Ag/H_2Pc/ITO/Ag$ device took the values of 1.02×10^{-3} to 1.20×10^{-3} A, for $Ag/H_2Pc/CuO_x/Ag$ device this obtained the values of 7.52×10^{-3} to 1.0×10^{-2} A.

Photocurrent values ($I_{ph}=I_{ill}$-I_{dark}) of $Ag/H_2Pc/ITO/Ag$ and $Ag/H_2Pc/CuO_x/Ag$ devices calculated between the light intensity of 20 and 100 mW.cm^{-2} at ± 3 V are given in Table 2. It is seen that I_{ph} values of $Ag/H_2Pc/ITO/Ag$ device at -3 V and 3 V took the values between 1.66×10^{-3} and 2.12×10^{-3}A and 2.46×10^{-3} and 2.69×10^{-3} A, respectively. At the same time, for $Ag/H_2Pc/CuO_x/Ag$ device, I_{ph} values at -3 V and 3 V were determined between 3.60×10^{-3} and 0.49×10^{-3} A and 3.58×10^{-3} and 0.16×10^{-3} A, respectively, and the alteration of I_{ph} as a function of light intensity at forward and reverse bias exhibited exponentially decreasing trend. Additionally, the highest I_{ph} values of $Ag/H_2Pc/ITO/Ag$ and $Ag/H_2Pc/CuO_x/Ag$ devices were obtained at forward and reverse bias under 80 mW.cm^{-2} and 20 mW.cm^{-2} light intensities, respectively. The heterojunctions reached their maximum photogenerated and saturated at these light intensities. Compared to the I_{ph} values, it is obtained that $Ag/H_2Pc/ITO/Ag$ device had higher values. The main reason for this can be attributed to the optical analyses showing that the H_2Pc/ITO heterojunction has higher α, k and lower E_g values than the H_2Pc/CuO_x heterojunction.

Photoresponsivity (R) is calculated from the ratio of the obtained photocurrent to incoming optical power with the equation of $R = I_{ph}/P_{inc}A$ [43], where P_{inc} is the light intensity and A (1.02×10^{-4} m^2) is the area of the active layer. While R values of $Ag/H_2Pc/ITO/Ag$ heterojunctions at – 3 V and 3 V applied potential took the values of 0.81–0.15 A W^{-1} and 1.28–0.24 A W^{-1}, respectively, for $Ag/H_2Pc/CuO_x/Ag$ these were 1.76–0.03 A W^{-1} and 1.75–0.01 A W^{-1} as listed in Table 2. The highest R values of both the heterojunctions under forward and reverse bias were obtained at 20 mW.cm^{-1} and they decreased with increasing the light intensity. The fact that the R values reach their highest value in a certain region and decrease in other light intensities can be explained by the decrease in absorption with the radial change of light intensity [58]. It may be noted that the obtained R values are higher than Co/CR/n-Si photodiodes [59] and p-Si/Fe(II)–polymeric complex/Au devices [60].

The percentage photosensitivity, $PS\%$, is determined via the equation of $PS\% = 100x(I_{ph} - I_d)/I_d$ [61–63] and I_d refers to the dark current. While the $PS\%$ values of $Ag/H_2Pc/ITO/Ag$ heterojunction varied between 91.59 and 92.24% at -3 V and 113.38 and 112.22% at 3 V, for $Ag/H_2Pc/CuO_x/Ag$ device these took values between 78.24 and 98.34% at -3 V and 120.10% and 100.88% at 3 V as shown in Table 2. The highest $PS\%$ value was obtained for $Ag/H_2Pc/ITO/Ag$ device at 3 V under 20 mW.cm^{-2} light intensity. This is also the region where the I_{ph} value is high. It is well known that oxygen plays an important role in the photosensitivity of diodes [64]. Thanks to the copper oxide layer, number of photogenerated electrons and holes significantly improved. This photoelectric advantage demonstrates that the optical transition works inside the nanolayers and supports an easy light collection procedure [65].

Specific detectivity (D^*) known as the detector capacity of weak light signals in photodiode is calculated via the equation of $D^* = R\sqrt{A}/(2qI_d)^{1/2}$ [66], where q refers to electron charge. D^* values were calculated for both the devices at ± 3 V potential range between 20 and 100 mW.cm^{-2} light intensity and are listed in Table 2. While the calculated D^* values for $Ag/H_2Pc/ITO/Ag$ device were found to be between 3.27×10^9 and 6.08×10^8 Jones at – 3 V and 5.11×10^9 and 9.58×10^8 Jones at 3 V, for $Ag/H_2Pc/CuO_x/Ag$ device this was obtained between 7.73×10^9 and 1.48×10^8 Jones at -3 V and 7.40×10^9 and 6.50×10^7 Jones at 3 V. It was obtained that D^* values decreased with the increase of the light intensity and the highest D^* values were found at 3 V under 20 mW.cm^{-2} for both the devices. Similar behaviour was observed for I_{ph} and R. Compared to the literature, it was found that the calculated D^* values were lower than ZnO/NiO [67] and InSe/PMItz [31] heterojunctions.

Photovoltaic regions of $Ag/H_2Pc/ITO/Ag$ and $Ag/H_2Pc/CuO_x/Ag$ devices are illustrated in Fig. 7 and photovoltaic parameters of the devices calculated between 20 and 100 mW.cm^{-2} light intensities are given in Table 2. The calculation

TABLE 2: Photodetector and photovoltaic parameters of Ag/H_2Pc/ITO/Ag and Ag/H_2Pc/CuO_x/Ag devices.

	Voltage (V)	Light intensity (mW cm^{-2})	I_{ph} (A)	R (A W^{-1})	PS%	D^* (Jones)
Ag/H_2Pc/ITO/Ag						
-3	20	1.66×10^{-3}	0.81	91.59	3.27×10^{9}	
	40	1.65×10^{-3}	0.40	91.64	1.62×10^{9}	
	60	1.64×10^{-3}	0.27	91.68	1.08×10^{9}	
	80	2.12×10^{-3}	0.26	89.28	1.04×10^{9}	
	100	1.53×10^{-3}	0.15	92.24	6.03×10^{8}	
3	20	2.62×10^{-3}	1.28	113.03	5.11×10^{9}	
	40	2.68×10^{-3}	0.65	113.31	2.61×10^{9}	
	60	2.62×10^{-3}	0.43	113.04	1.7×10^{9}	
	80	2.69×10^{-3}	0.33	113.38	1.31×10^{9}	
	100	2.46×10^{-3}	0.24	112.22	9.58×10^{8}	
Ag/H_2Pc/CuO_x/Ag						
-3	20	3.60×10^{-3}	1.76	78.24	7.73×10^{9}	
	40	3.32×10^{-3}	0.81	79.96	3.56×10^{9}	
	60	2.55×10^{-3}	0.42	84.60	1.83×10^{9}	
	80	0.27×10^{-3}	0.03	98.34	$1.48\times\times10^{8}$	
	100	0.49×10^{-3}	0.04	97.06	2.09×10^{8}	
3	20	3.58×10^{-3}	1.75	120.10	7.40×10^{9}	
	40	3.29×10^{-3}	0.80	118.46	3.40×10^{9}	
	60	2.25×10^{-3}	0.37	112.65	1.55×10^{9}	
	80	1.01×10^{-3}	0.12	105.68	5.24×10^{9}	
	100	0.16×10^{-3}	0.01	100.88	6.50×10^{7}	

Light intensity (mW cm^{-2})	I_{sc} (A)	I_{mpp} (A)	V_{oc} (V)	V_{mpp} (V)	FF%	η%
Ag/H_2Pc/ITO/Ag						
20	2.47×10^{-3}	1.22×10^{-3}	2.0×10^{-2}	1.10×10^{-2}	27.17	6.55×10^{-2}
40	1.75×10^{-3}	0.9×10^{-3}	1.5×10^{-2}	0.83×10^{-2}	28.68	1.84×10^{-2}
60	2.28×10^{-3}	1.2×10^{-3}	1.9×10^{-2}	0.98×10^{-2}	27.15	1.91×10^{-2}
80	2.45×10^{-3}	1.4×10^{-3}	2.1×10^{-2}	1.07×10^{-2}	29.12	1.83×10^{-2}
100	2.82×10^{-3}	1.5×10^{-3}	2.2×10^{-2}	1.18×10^{-2}	28.53	1.73×10^{-2}
Ag/H_2Pc/CuO_x/Ag						
20	1.91×10^{-3}	1.01×10^{-3}	1.61×10^{-2}	0.84×10^{-2}	27.59	4.14×10^{-2}
40	2.11×10^{-3}	1.16×10^{-3}	1.94×10^{-2}	1.01×10^{-2}	28.34	2.83×10^{-2}
60	2.27×10^{-3}	1.26×10^{-3}	2.09×10^{-2}	1.08×10^{-2}	28.68	2.21×10^{-2}
80	2.54×10^{-3}	1.47×10^{-3}	2.51×10^{-2}	1.25×10^{-2}	28.82	2.24×10^{-2}
100	2.29×10^{-3}	1.28×10^{-3}	2.46×10^{-2}	1.27×10^{-2}	28.87	1.59×10^{-2}

of the power conversion efficiency (η%) is performed as follows [68], $\eta\% = (V\text{oc}.I\text{sc}/A.\text{Pin}).\text{FF}x100$, where Pin is the power of incident light per unit area and FF is the fill factor. Percentage fill factor, FF%, is calculated with the expression of $\text{FF}\% = (\text{I}_{\text{mpp}}\text{V}_{\text{mpp}}/\text{I}_{\text{sc}}\text{V}_{\text{oc}})\text{x}100$, where V_{oc} is the open circuit voltage, I_{sc} is the short circuit current and I_{mpp} and V_{mpp} are the current and voltage at the maximum power point (mmp), respectively. V_{oc} values of Ag/H_2Pc/ITO/Ag and Ag/H_2Pc/CuO_x/Ag devices took the values between 1.5×10^{-2} and 2.2×10^{-2} V and 1.6×10^{-2} and 2.5×10^{-2} V, respectively. Besides, the highest value of Ag/H_2Pc/ITO/Ag device was obtained at 100 mW.cm^{-2} light intensity, while for Ag/H_2Pc/CuO_x/Ag device this was obtained at 80 mW.cm^{-2} light intensity. It might also be noted that increasing the light intensity led to increase of V_{oc} values of both the heterojunctions. In general, it is seen that the V_{oc} values of the Ag/H_2Pc/ITO/Ag device were higher than that of the Ag/H_2Pc/CuO_x/Ag device. The I_{sc} values of the Ag/H_2Pc/ITO/Ag device took values between 1.75×10^{-3} and 2.82×10^{-3} A with the highest value at 100 mW.cm^{-2}, while that of the Ag/H_2Pc/CuO_x/Ag device were between 1.91×10^{-3} and 2.54×10^{-3} A with the highest value at 80 mW.cm^{-2}. It is also seen that similar to $V_{oc,}$ I_{sc} values increased with the increase of light intensity in both the devices, and this is typical photodiode behaviour. In addition, while the highest $FF\%$ value was 29.12% at 80 mW.cm^{-2} light intensity Ag/H_2Pc/ITO/Ag device, it was measured as 28.87% at 100 mW.cm^{-2} light intensity at Ag/

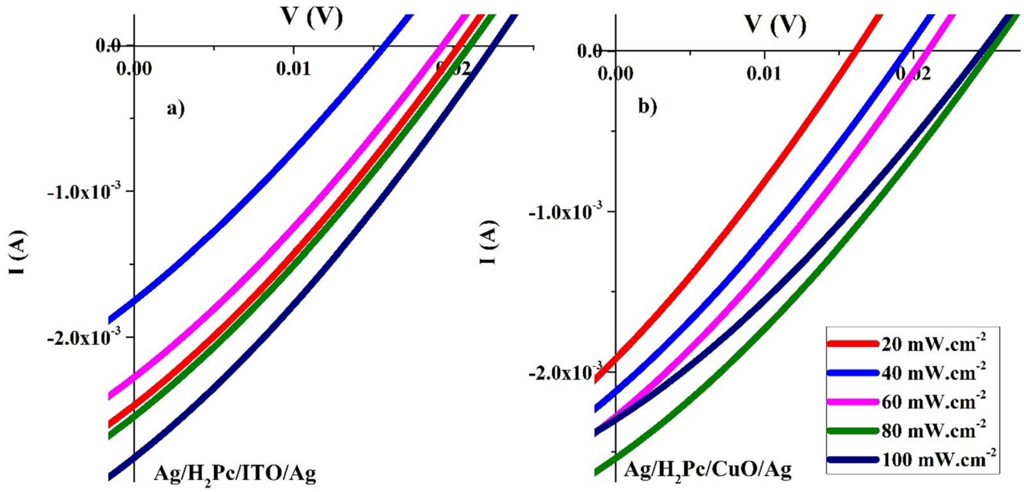

Figure 7: Photovoltaic regions of (a) Ag/H_2Pc/ITO/Ag (b) Ag/H_2Pc/CuO_x/Ag devices.

H_2Pc/CuO_x/Ag device. The η% values of the Ag/H_2Pc/ITO/Ag heterojunction were between 6.55×10^{-2} and 1.73×10^{-2}, while the η% values of the Ag/H_2Pc/CuO_x/Ag heterojunction were between 4.14×10^{-2} and 1.59×10^{-2}. In both the heterojunctions, the maximum η% value was observed at 20 mW.cm^{-2} light intensity. In general, η% values are found to be smaller compared with Pc-based devices in the literature [69]. It is seen that η% values decrease with increasing light intensity in both the devices. In general, the trend of the photodetector parameters against the light was also observed in the η% values. The radial change of light intensity with the increase of light intensity caused a decrease in η% values due to the decrease in absorption. At 20 mW.cm^{-2} light intensity, the maximum η% value of Ag/H_2Pc/ITO/Ag heterojunction is higher than Ag/H_2Pc/CuO_x/Ag heterojunction. This may be related to the high recombination between the CuO_x and the H_2Pc layer, as well as the high series resistance value. The fact that the V_{oc} values of the Ag/H_2Pc/ITO/Ag heterojunction are higher than that of the Ag/H_2Pc/CuO_x/Ag heterojunction is also the reason for high η% values. In addition, the reverse saturation current values of the Ag/H_2Pc/CuO_x/Ag heterojunction are higher than that of the Ag/H_2Pc/ITO/Ag heterojunction, which is the reason why the η% value is low. In addition to the high series resistance, the excess of leakage currents is one of the reasons for the decrease in efficiency in solar cells.

Conclusion

The modified H_2Pc organic semiconductors were successfully grown on ITO/glass and CuO_x/ITO/glass substrates. The energy band gap values of H_2Pc deposited on ITO/glass and CuO_x/ITO/glass were obtained as 2.77 and 2.66 eV, respectively. It is also obtained that optical parameters (α, R, k, n, σ, ε_i, ε_r and $\varepsilon_i/\varepsilon_r$) of H_2Pc/CuO_x/ITO/glass heterojunction were quite higher than that of H_2Pc/ITO/glass heterojunctions. Electrical analyses of Ag/H_2Pc/ITO/Ag and Ag/H_2Pc/CuO_x/Ag devices were performed under dark and several light intensities. It revealed that both the devices were sensitive to the light and exhibited rectifier characteristic especially in the low voltage region. Diode parameters (n, ϕ_b, R_s and I_0) of both the heterojunctions were determined by different methods (traditional method, Cheung&Cheung method and Ohm's law). In addition, the photodetector and photovoltaic parameters of both the devices were investigated at different light intensities. Consequently, it can be stated that both the devices having organic-based thin film technology might contribute novelty to the field of optoelectronic applications.

Materials and methods

The heterojunctions were fabricated on properly cleaned ITO/glass substrates with the following steps.

Synthesis of modified H_2Pc organic molecule

In the synthetic approach, firstly, compound 3 [see Fig. 8(a)] was synthesised by the SNAr-type reaction and then metal-free phthalocyanines are prepared from phthalonitriles in the presence of basic catalyst and synthesis and spectroscopic details of the compounds can be found in the literature [70].

Growing of CuO_x thin film

CuO_x thin film deposition on ITO/glass substrates was performed using a two-inch Cu (99.999% purity) magnetron target powered by the RF generator. Nanovak magnetron sputter system (Model:NVTS-400) was pumped down until it reached to 1×10^{-5} Torr base pressure. Deposition rate of Cu material

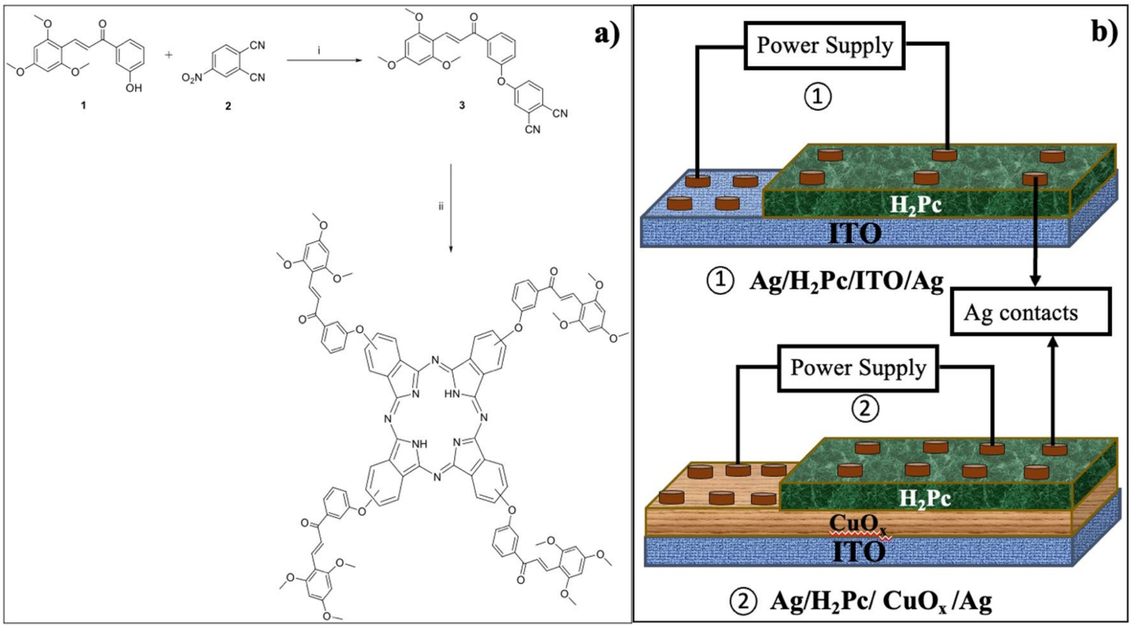

Figure 8: (a) Synthesis of modified H_2Pc organic molecule. (b) Schematic views of Ag/H_2Pc/ITO/Ag and Ag/H_2Pc/CuO_x/Ag devices.

was kept 1 Å/s by applying 65 W sputter power and 5 mTorr Ar gas injection under 3×10^{-3} Torr vacuum conditions. After reaching approximately 350 nm thickness, Cu film was annealed with 30 mTorr oxygen injection at 473 K during 30 min under high vacuum conditions.

Growing of modified H_2Pc thin film and fabrication of heterojunctions

The modified H_2Pc organic molecule was deposited on ITO/glass and CuO_x/ITO/glass surfaces as a thin film via the thermal evaporation method under high vacuum conditions. H_2Pc was placed in a molybdenum boat and evaporated controllably via the applied voltage at room temperature by employing Vaksis (PVD-MT/2M2T) thermal evaporator system. The working pressure of the deposition system was approximately 2×10^{-6} Torr. After ≈50 nm H_2Pc thin film was deposited on the ITO/glass and CuO_x/ITO/glass surface, a mask which has 0.77 mm diameter circular holes was applied to the top of the films. Thereafter, Ag contacts were grown on H_2Pc/ITO and H_2Pc/CuO_x surfaces via the thermal evaporation method, and Ag/H_2Pc/ITO/Ag and Ag/H_2Pc/CuO_x/Ag devices were fabricated as demonstrated in Fig. 8b.

Characterisation of the heterojunctions

Bruker D8 Advance X-ray diffractometer (XRD) was used to analyse the phase structure of CuO_x/ITO over a 10° to 70° range. The surface morphologies and the elemental compositions of the CuO_x were determined via FEI Quanta FEG 250 Scanning Electron Microscope (SEM) equipped with Energy-dispersive X-ray spectrometry (EDX). Optical characterisation was performed via a Hach DR6000 model UV–vis spectrometer. Electrical characteristics of each heterojunction were examined under dark and illuminations between 20 mW.cm^{-2} and 100 mW.cm^{-2} via the FYTRONIX Solar Simulator LSS 900 I–V Characterisation System.

Author contributions

All authors contributed to the study conception and design. FU: drafting, coating of organic thin films and generation of heterojunctions, electrical analysis, conceptualisation, formal analysis and writing. SA: writing, editing, design and optical analysis. MSK: production of CuO_x thin film, writing and editing. MMK: I–V measurement, writing and editing. TA: synthesis of organic compound and writing. BC: I–V measurement and writing. MG: SEM and EDX measurement and writing. All authors read and approved the final manuscript.

Funding

There is no funding for this work.

Data availability

All data that support the findings of this study are included within the article (and any supplementary files).

Declarations

Conflict of interest The authors declare that they have no conflicts of interest.

References

1. H. Bronstein et al., The role of chemical design in the performance of organic semiconductors. Nat. Rev. Chem. **4**(2), 66–77 (2020)
2. V.V. Brus et al., Electrical and photoelectrical properties of P3HT/n-Si hybrid organic–inorganic heterojunction solar cells. Org. Electron. **14**(11), 3109–3116 (2013)
3. S. Demirezen et al., Electrical characteristics and photosensing properties of Al/symmetrical CuPc/p-Si photodiodes. J. Mater. Sci.: Mater. Electron. **33**(26), 21011–21021 (2022)
4. M. Zurnacı et al., Synthesis of a new 1,3,4-thiadiazole-substituted phenanthroimidazole derivative, its growth on glass/ITO as a thin film and analysis of some surface and optoelectronic properties. New J. Chem. **45**(48), 22678–22690 (2021)
5. F. Unal et al., Synthesis and optoelectronic characterization of coronene/CdO self-powered photodiode. J. Mater. Sci.: Mater. Electron. (2022). https://doi.org/10.1007/s10854-022-09237-y
6. M.S. Kurt et al., Optical and electrical characterization of a ZnO/coronene-based hybrid heterojunction photodiode. J. Electron. Mater. **51**, 6846–6857 (2022)
7. S. Aktas et al., Fabrication and morphological, optical, and electrical characterisation of Cu-doped ZnO nanorod/coronene nanowire hybrid heterojunctions. Phys. Scr. (2022). https://doi.org/10.1088/1402-4896/ac9e7c
8. S. Li et al., A self-powered solar-blind photodetector with large Voc enhancing performance based on the PEDOT:PSS/Ga2O3 organic–inorganic hybrid heterojunction. J. Mater. Chem. C **8**(4), 1292–1300 (2020)
9. F.A. Alawainati et al., Nonlinear optical properties of novel metallophthalocyanines. J. Appl. Spectrosc. **88**(5), 951–957 (2021)
10. Z. Biyiklioglu et al., Comparative nonlinear optics and optical limiting properties of metallophthalocyanines. Inorg. Chim. Acta **486**, 345–351 (2019)
11. M. Demirol et al., Synthesis and photodiode properties of chalcone substituted metallo-phthalocyanine. J. Mol. Struct. **1219**, 128571 (2020)
12. N. Mutz et al., Excited-state charge transfer enabling MoS2/phthalocyanine photodetectors with extended spectral sensitivity. J. Phys. Chem. C **124**(5), 2837–2843 (2020)
13. T. Paltrinieri et al., Understanding photocapacitive and photofaradaic processes in organic semiconductor photoelectrodes for optobioelectronics. Adv. Func. Mater. **31**(16), 2010116 (2021)
14. S. Dolai et al., Cupric oxide (CuO) thin films prepared by reactive dc magnetron sputtering technique for photovoltaic application. J. Alloy Compd. **724**, 456–464 (2017)
15. B.K. Meyer et al., Binary copper oxide semiconductors: From materials towards devices. Phys. Status Solidi B **249**(8), 1487–1509 (2012)
16. A.S. Zoolfakar et al., Nanostructured copper oxide semiconductors: a perspective on materials, synthesis methods and applications. J. Mater. Chem. C **2**(27), 5247–5270 (2014)
17. V.-H. Castrejón-Sánchez et al., Thermal oxidation of copper over a broad temperature range: towards the formation of cupric oxide (CuO). Mater. Res. Express **6**(7), 075909 (2019)
18. C. Abinaya et al., The effect of post-deposition annealing conditions on structural and thermoelectric properties of sputtered copper oxide films. RSC Adv. **10**(49), 29394–29401 (2020)
19. F.A. Akgul et al., Influence of thermal annealing on microstructural, morphological, optical properties and surface electronic structure of copper oxide thin films. Mater. Chem. Phys. **147**(3), 987–995 (2014)
20. D.S. Murali, A. Subrahmanyam, Synthesis of low resistive p type Cu4O3 thin films by DC reactive magnetron sputtering and conversion of Cu4O3 into CuO by laser irradiation. J. Phys. D **49**(37), 375102 (2016)
21. D. Dwivedi, B. Singh, M. Dubey, Structural and optical investigations of Cd1– xZnxTe thin film. J. Non-Cryst. Solids **356**(31–32), 1563–1568 (2010)
22. S. Aktas et al., Investigation of fundamental electrical and optoelectronic properties of an organic- and carbon-based MnPc/GC photodiode with high photosensitivity. Phys. Scr. **98**(9), 095504 (2023)
23. J. Tauc, Optical properties and electronic structure of amorphous Ge and Si. Mater. Res. Bull. **3**(1), 37–46 (1968)
24. V. Bilgin et al., The effect of substrate temperature on the structural and some physical properties of ultrasonically sprayed CdS films. Mater. Chem. Phys. **94**(1), 103–108 (2005)
25. F. Atay, O. Gultepe, Structural, optical and surface properties of sol–gel-derived boron-doped ZnO films for photocatalytic applications. Appl. Phys. A **128**(2), 99 (2022)
26. Ü. Fatih, Comparison of optical properties of Cu- and In-doped CdO thin films having low dielectric loss. J. Mater. Electron. Devices **1**(1), 67–72 (2023)
27. F. Unal, Determination of the basic optical parameters of CdX (X= Se, S) thin films prepared with low concentration precursor solutions. J. Charact. **3**(1), 30–36 (2023)
28. S. Aktas, Investigation and comparison of optical properties of CdO and CdGaO transparent conductive metal oxide thin films. J. Mater. Electron. Devices **1**(1), 2–17 (2023)
29. M. Engin et al., Growth and characterization of Zn-incorporated copper oxide films. J. Electron. Mater. **38**(6), 787–796 (2009)
30. M. Engin et al., Growth and characterization of Zn-incorporated copper oxide films. J. Electron. Mater. **38**, 787–796 (2009)

31. Ü. Fatih, et al., Electrical properties of InSe/PMItz nanocomposite thin films. J. Mater. Electron. Devices **3**(1) (2022)
32. A. Farag, I. Yahia, Rectification and barrier height inhomogeneous in Rhodamine B based organic Schottky diode. Synth. Met. **161**(1–2), 32–39 (2011)
33. K. Saron et al., Interface properties determined the performance of thermally grown GaN/Si heterojunction solar cells. Sol. Energy **98**, 485–491 (2013)
34. Z. Xu et al., Growth of GaN on Si (111): Surfaces and crystallinity of the epifilms and the transport behavior of GaN/Si heterojunctions. J. Appl. Phys. **110**(9), 093514 (2011)
35. M.S. Kurt et al., Optical and electrical characterization of a ZnO/coronene-based hybrid heterojunction photodiode. J. Electron. Mater. **51**(12), 6846–6857 (2022)
36. S.M. Sze, K.K.N., *p-n Junctions*, in *Physics of Semiconductor Devices* (Wiley, New Jersey, 2006, pp. 77–133)
37. S.K. Cheung, N.W. Cheung, Extraction of Schottky diode parameters from forward current-voltage characteristics. Appl. Phys. Lett. **49**(2), 85–87 (1986)
38. H. Çetinkaya et al., Photovoltaic characteristics of Au/PVA (Bi-doped)/n-Si Schottky barrier diodes (SBDs) at various temperatures. Curr. Appl. Phys. **13**(6), 1150–1156 (2013)
39. S. Tan et al., Electrical characterizations of Au/ZnO/n-GaAs Schottky diodes under distinct illumination intensities. J. Mater. Sci.: Mater. Electron. **27**(8), 8340–8347 (2016)
40. F. Ünal, Investigation of diode parameters of photoconductive and photovoltaic p-type Si/Ge-doped WOx heterojunction. J. Electron. Mater. **51**(11), 6397–6409 (2022)
41. S.S. Li, Scattering mechanisms and carrier mobilities in semiconductors, in *Semiconductor Physical Electronics*. (Springer, 2006), pp.211–245
42. E.H. Rhoderick, Metal-semiconductor contacts. IEE Proc. I **129**(1), 1 (1982)
43. S. Aktas, Electrical characterisation of photosensitive Si/W–Ge oxide composite heterojunction. Opt. Mater. **132**, 112839 (2022)
44. F. Unal, M.S. Kurt, S. Durdu, Investigation of the effect of light on the electrical parameters of Si/TiO2 heterojunctions produced by anodic oxidation on p-type Si wafer. J. Mater. Sci.: Mater. Electron. **33**(19), 15834–15847 (2022)
45. H.E. Lapa et al., Effect of illumination on electrical parameters of Au/(P3DMTFT)/n-GaAs Schottky barrier diodes. Indian J. Phys. **94**(12), 1901–1908 (2020)
46. F. Yakuphanoglu, Controlling of silicon–insulator–metal junction by organic semiconductor polymer thin film. Synth. Met. **160**(13), 1551–1555 (2010)
47. H. Seymen et al., Effect of illumination intensity on the electrical characteristics of Au//SiO2/n-type Si structures with GO and P3C4MT interface layer. J. Mater. Sci.: Mater. Electron. **33**(24), 19656–19666 (2022)
48. W. Mönch, Barrier heights of real Schottky contacts explained by metal-induced gap states and lateral inhomogeneities. J. Vac. Sci. Technol. B **17**(4), 1867–1876 (1999)
49. K. Akkiliç, M.E. Aydin, A. Türüt, The effect of series resistance on the relationship between barrier heights and ideality factors of inhomogeneous Schottky barrier diodes. Phys. Scr. **70**(6), 364 (2004)
50. R.F. Schmitsdorf, T.U. Kampen, W. Mönch, Explanation of the linear correlation between barrier heights and ideality factors of real metal-semiconductor contacts by laterally nonuniform Schottky barriers. J. Vac. Sci. Technol. B **15**(4), 1221–1226 (1997)
51. Ş Altındal, Ö. Sevgili, Y. Azizian-Kalandaragh, A comparison of electrical parameters of Au/n-Si and Au/(CoSO4–PVP)/n-Si structures (SBDs) to determine the effect of (CoSO4–PVP) organic interlayer at room temperature. J. Mater. Sci.: Mater. Electron. **30**(10), 9273–9280 (2019)
52. Fatih, Ü., *Investigation Of Some Optical And Electrical Properties Of InSe Thin Film, a Window Layer for Photovoltaic Cell Growth on Glass/GaSe Substrate by M-CBD Method.* Karadeniz Fen Bilimleri Dergisi. **11**(1): p. 297–306.
53. B. Gunduz, I.S. Yahia, F. Yakuphanoglu, Electrical and photoconductivity properties of p-Si/P3HT/Al and p-Si/P3HT:MEH-PPV/Al organic devices: Comparison study. Microelectron. Eng. **98**, 41–57 (2012)
54. E. Yükseltürk et al., Illumination and voltage effects on the forward and reverse bias current–voltage (I-V) characteristics in In/In2S3/p-Si photodiodes. J. Mater. Sci.: Mater. Electron. **32**(17), 21825–21836 (2021)
55. H. Bayhan, M. Bayhan, A simple approach to determine the solar cell diode ideality factor under illumination. Sol. Energy **85**(5), 769–775 (2011)
56. Ü. Fatih, and S. Aktaş, *Işığa Duyarlı n-tipi Katkılı Metal oksit/p-tipi Si Heteroekleminin Elektriksel Karakterizasyonu.* J. Inst. Sci. Technol. **12**(3), 1506–1517.
57. M. Saad, A. Kassis, Effect of interface recombination on solar cell parameters. Sol. Energy Mater. Sol. Cells **79**(4), 507–517 (2003)
58. A. Patel et al., Fabrication, photoresponse and temperature dependence of n-VO2/n-MoSe2 heterojunction diode. Superlattices Microstruct. **130**, 160–167 (2019)
59. A. Kocyigit et al., The light detection performance of the congo red dye in a Schottky type photodiode. Chem. Phys. Lett. **800**, 139673 (2022)
60. B. Gündüz et al., The photo-electrical properties of the p-Si/Fe(II)–polymeric complex/Au diode. Synth. Met. **184**, 73–82 (2013)
61. P. Vivek et al., Fabrication of illumination-dependent Cu/p-Si Schottky barrier diodes by sandwiching MoO3 nanoplates as an interfacial layer via JNSP technique. J. Electron. Mater. **49**(7), 4249–4264 (2020)

62. V. Balasubramani et al., Colossal photosensitive boost in Schottky diode behaviour with Ce-V2O5 interfaced layer of MIS structure. Sens. Actuators A **315**, 112333 (2020)
63. C.A. Canbay, O. Karaduman, The photo response properties of shape memory alloy thin film based photodiode. J. Mol. Struct. **1235**, 130263 (2021)
64. B. Yuan et al., High photosensitivity and low dark current of photoconductive semiconductor switch based on ZnO single nanobelt. Solid-State Electron. **55**(1), 49–53 (2011)
65. W. Luo et al., Room-temperature single-photon detector based on single nanowire. Nano Lett. **18**(9), 5439–5445 (2018)
66. B. Murali, S.B. Krupanidhi, Transport properties of CuIn1−xAlxSe2/AZnO heterostructure for low cost thin film photovoltaics. Dalton Trans. **43**(5), 1974–1983 (2014)
67. L. Zheng et al., Large scale, highly efficient and self-powered UV photodetectors enabled by all-solid-state n-TiO 2 nanowell/p-NiO mesoporous nanosheet heterojunctions. J. Mater. Chem. C **4**(42), 10032–10039 (2016)
68. A.Q. Alosabi et al., Characterization and photovoltaic performance analysis of Na2Pc/p-Si heterojunction solar cell. J. Mater. Sci.: Mater. Electron. **33**(33), 25329–25341 (2022)
69. G.K. Karaoğlan et al., Synthesis, characterization, electrochemical, spectroelectrochemical and dye-sensitized solar cell properties of phthalocyanines containing carboxylic acid anchoring groups as photosensitizer. Dyes Pigm. **204**, 110390 (2022)
70. T. Arslan, Design, synthesis of novel peripherally tetra-chalcone substituted phthalocyanines and their inhibitory effects on acetylcholinesterase and carbonic anhydrases (hCA I and II). J. Organomet. Chem. **951**, 122021 (2021)